- Supplementary Material -

Thermodynamically stable and Metastable Coordination Polymers Synthesized from Solution and the Solid State

Tristan Neumann, Gianpiero Gallo, Inke Jess, Robert E. Dinnebier and Christian Näther

Content

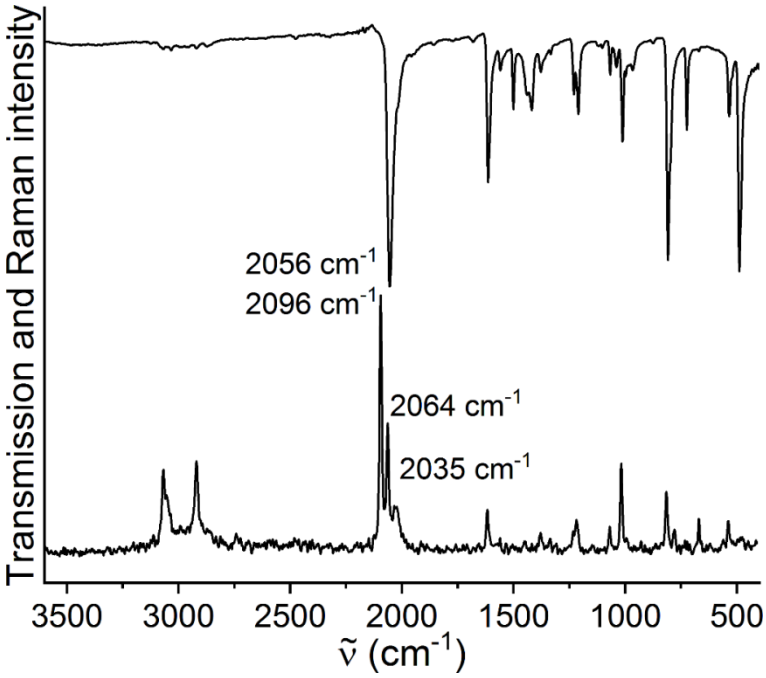

Figure S1. IR- (top) and Raman spectra (bottom) of **1-Fe** with the values for the C-N stretching vibrations.

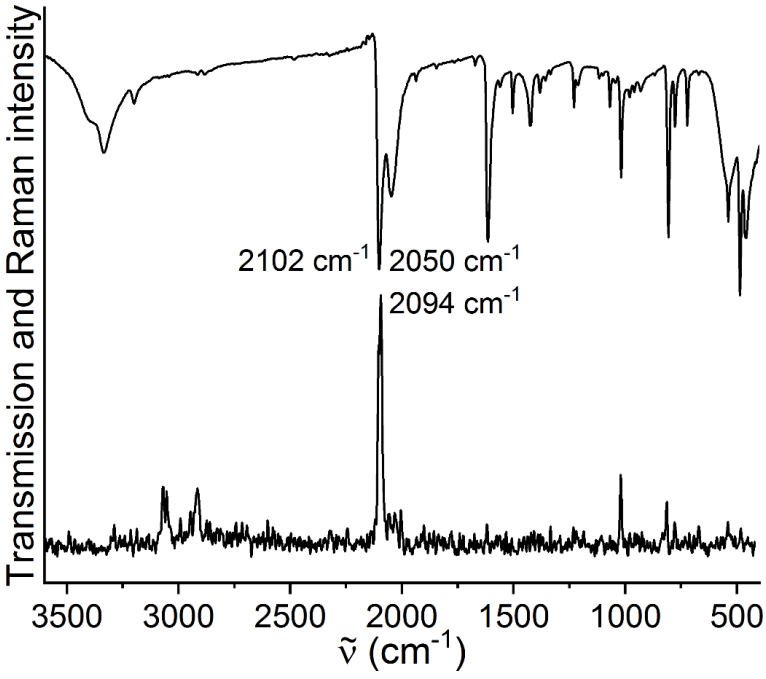

Figure S2. IR- (top) and Raman spectra (bottom) of **2-Fe/H_2O** with the values for the C-N stretching vibrations.

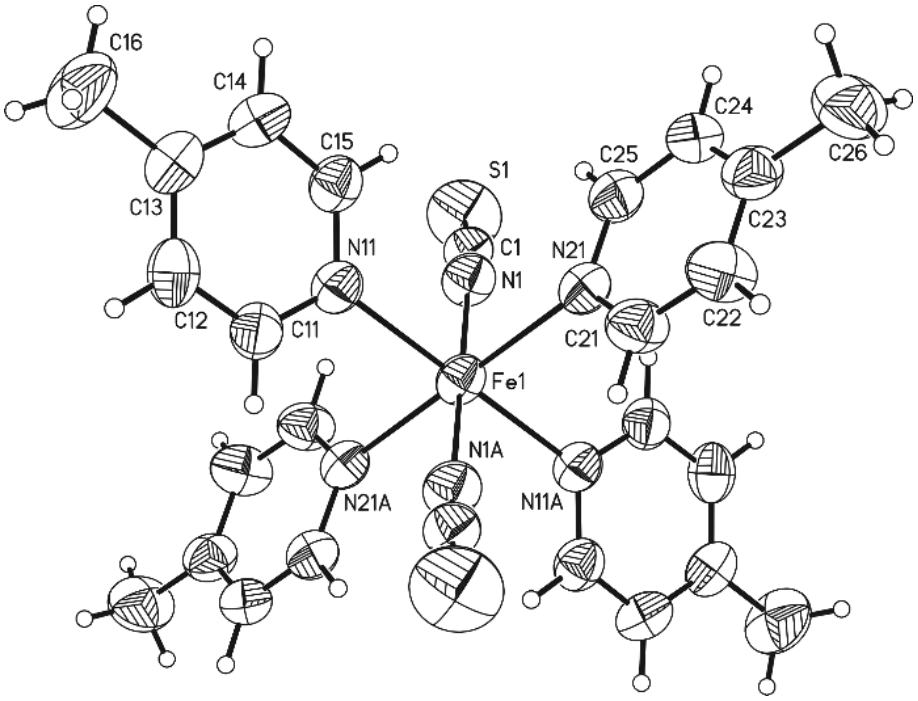

Figure S3. View of a discrete complex in the crystal structure of **1-Fe** with labeling and displacement ellipsoids drawn with 50% probability.

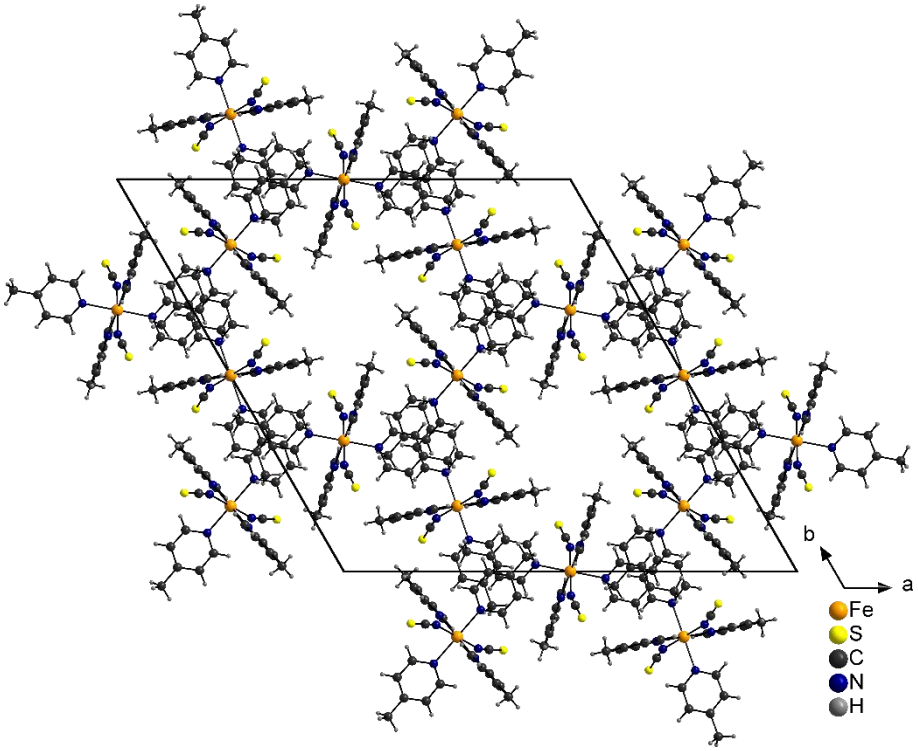

Figure S4. Crystal structure of **1-Fe** with view along the crystallographic *c*-axis. The disordered solvent molecules are located in channels along this axis.

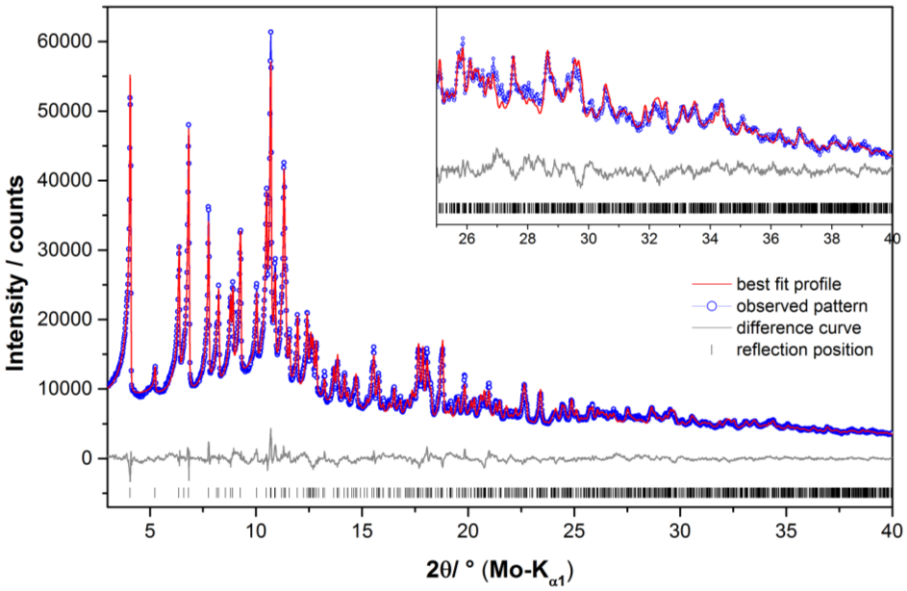

Figure S5. Rietveld plot of **2-Fe/H_2O**. The observed pattern (blue circles) was measured in Debye-Scherrer geometry, the best Rietveld fit profiles (red line), the difference curve between the observed and the calculated profiles (grey line) and calculated peak positions for $Fe(NCS)_2(4\text{-picoline})_2(H_2O)_2$ (black) are shown. The high angle part starting at 25° in 2θ is enlarged for clarity.

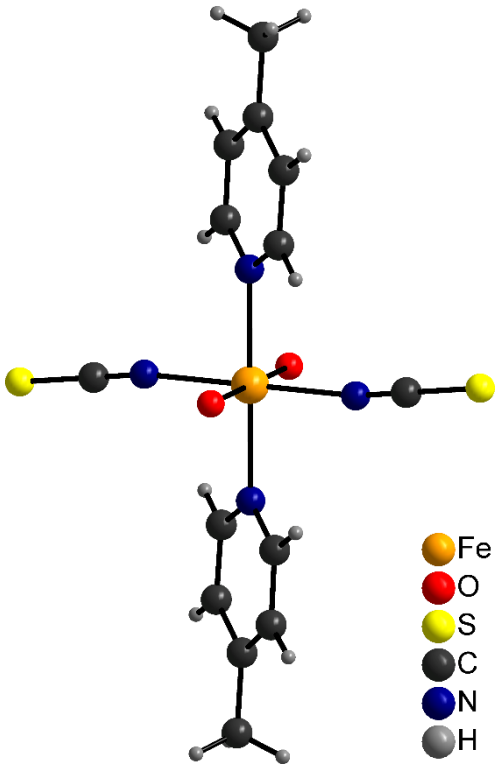

Figure S6. View of a discrete complex in the crystal structure of **2-Fe/H_2O**.

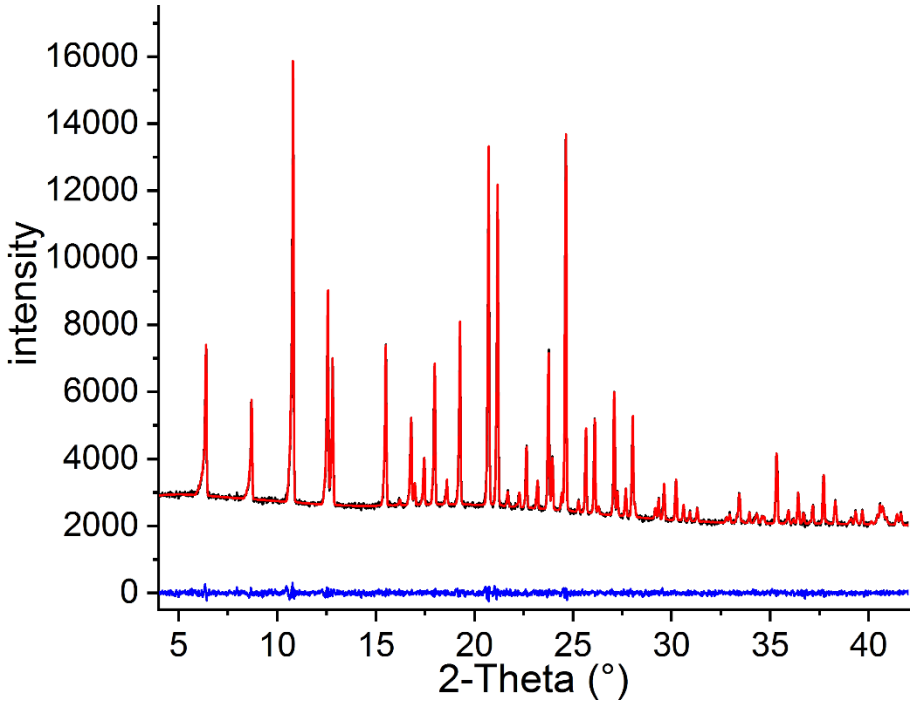

Figure S7. Experimental XRPD pattern of **1-Fe** measured with Cu-Kα1 radiation. (black), Pawley fit starting from the single crystal data (red) and difference curve (blue).

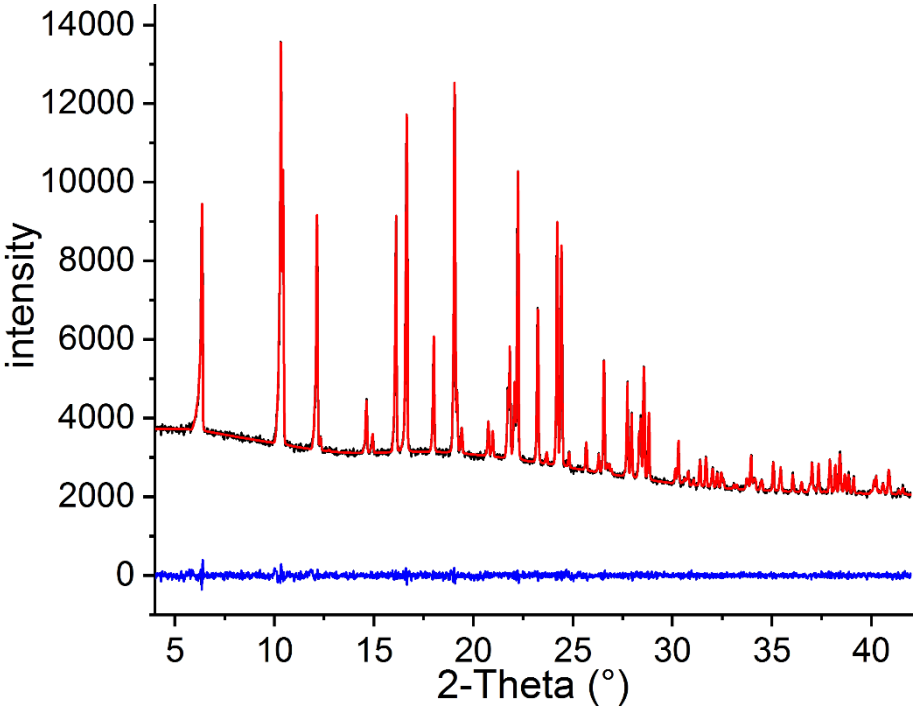

Figure S8. Experimental XRPD pattern of $Fe(NCS)_2(4\text{-picoline})_4 \cdot$ 4-picoline (black), Pawley fit starting from the single crystal data retrieved from literature (red) and the difference curve (blue).

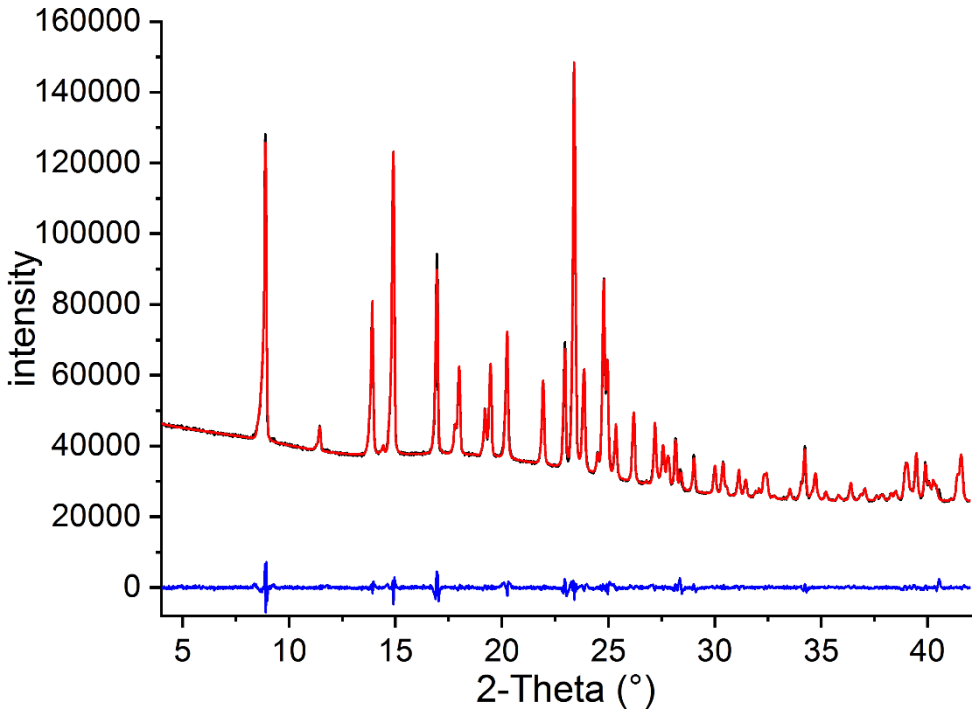

Figure S9. Experimental XRPD pattern of **2-Fe/H_2O** (black), Pawley fit (red) and the difference curve (blue).

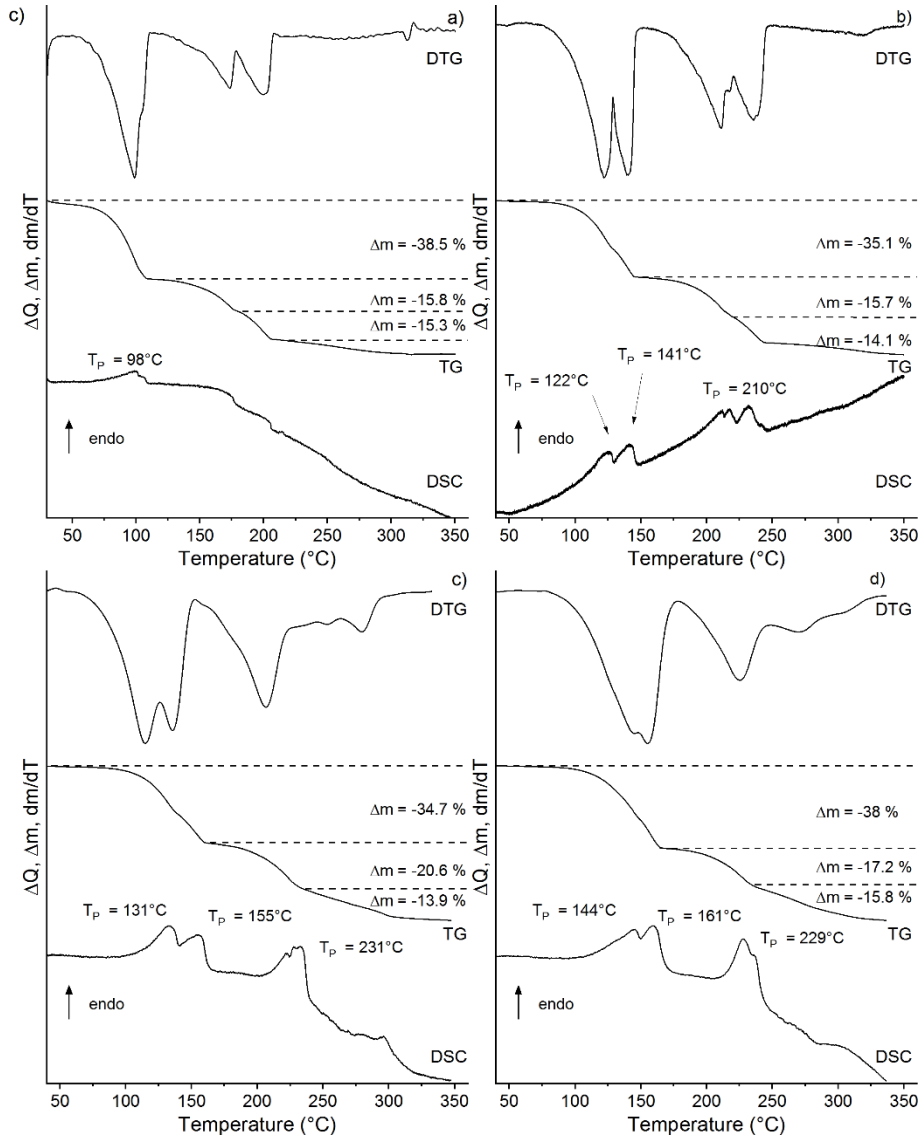

Figure S10. DTG, TG and DSC curves for **1-Fe** at a) 0.2°C/min, b) 1°C/min, c) 4°C/min and d) 8°C/min.

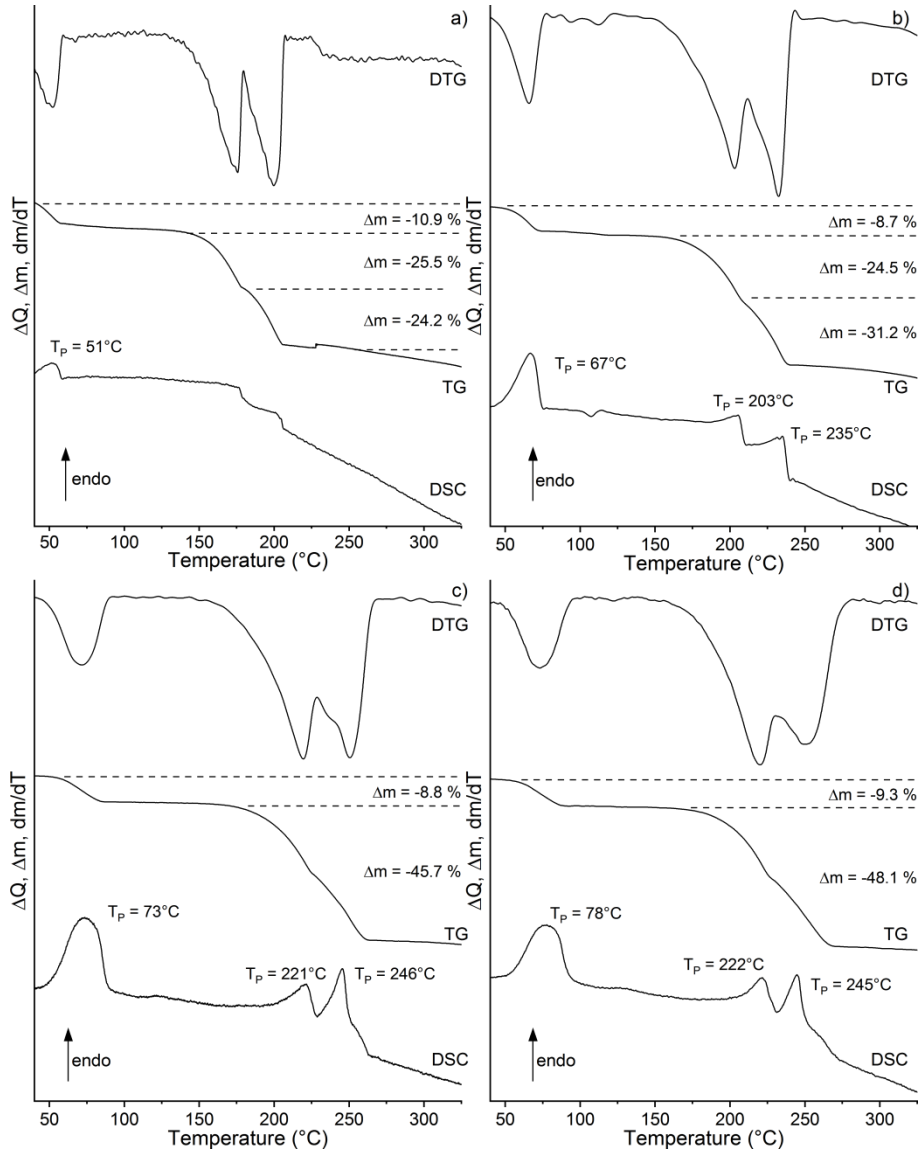

Figure S11. DTG, TG and DSC curves for **2-Fe/H_2O** at a) 0.2°C/min, b) 1°C/min, c) 4°C/min and d) 8°C/min.

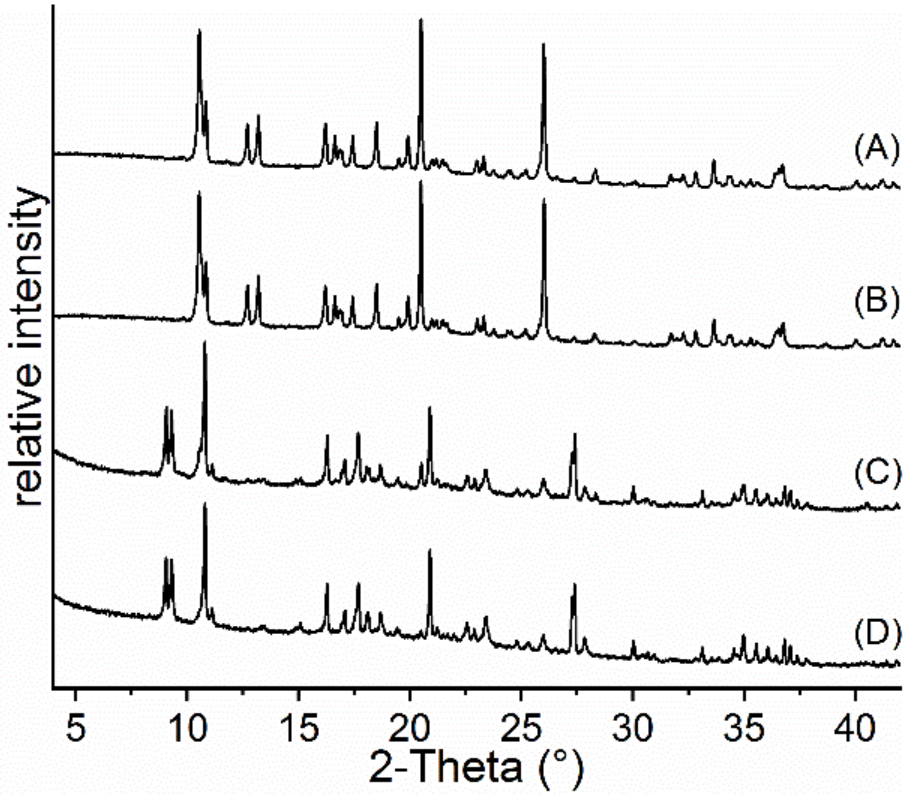

Figure S12. XRPD pattern of the residues obtained at the first (A and B) and the second mass loss (C and D) in the TG measurements of **2-Fe/H_2O** and **1-Fe** measured with Cu-Kα_1 radiation.

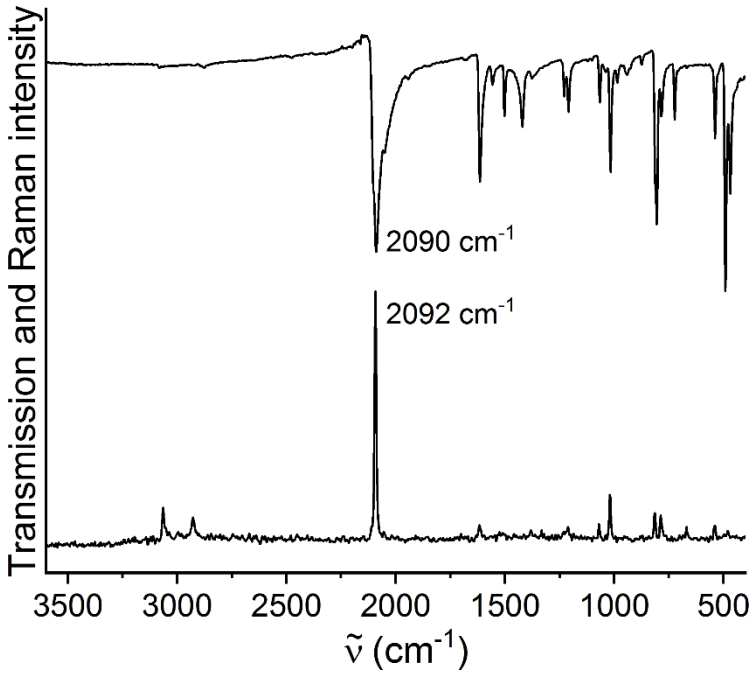

Figure S13. IR- (top) and Raman-spectra (bottom) of **2-Fe/I** with the values for the C-N stretching vibrations.

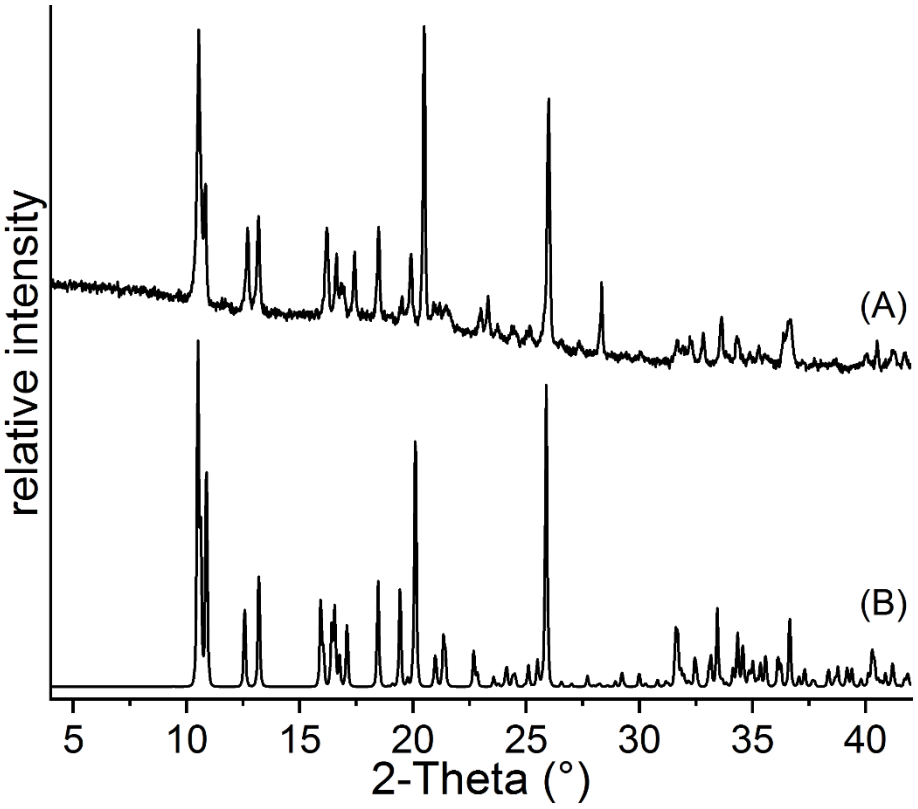

Figure S14. Experimental XRPD pattern for **2-Fe/I** measured with Cu-Kα_1 radiation and calculated pattern for $[Cd(NCS)_2(4\text{-picoline})_2]_n$ retrieved from literature.

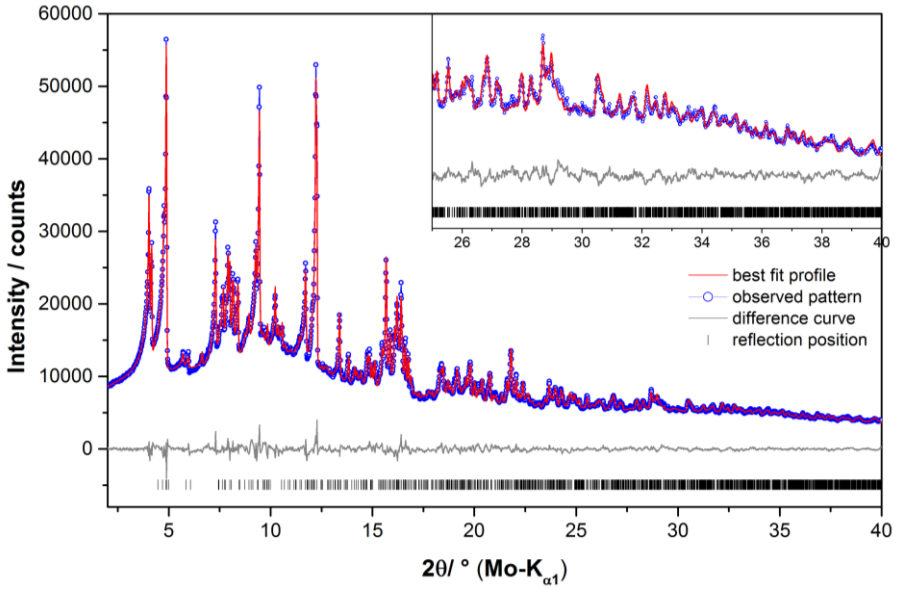

Figure S15. Rietveld plot of **2-Fe/I**. The observed pattern (circles) measured in Debye-Scherrer geometry, the best Rietveld fit profiles (line) and the difference curve between the observed and the calculated profiles (below) are shown. The high angle part starting at 25° in 2θ is enlarged for clarity.

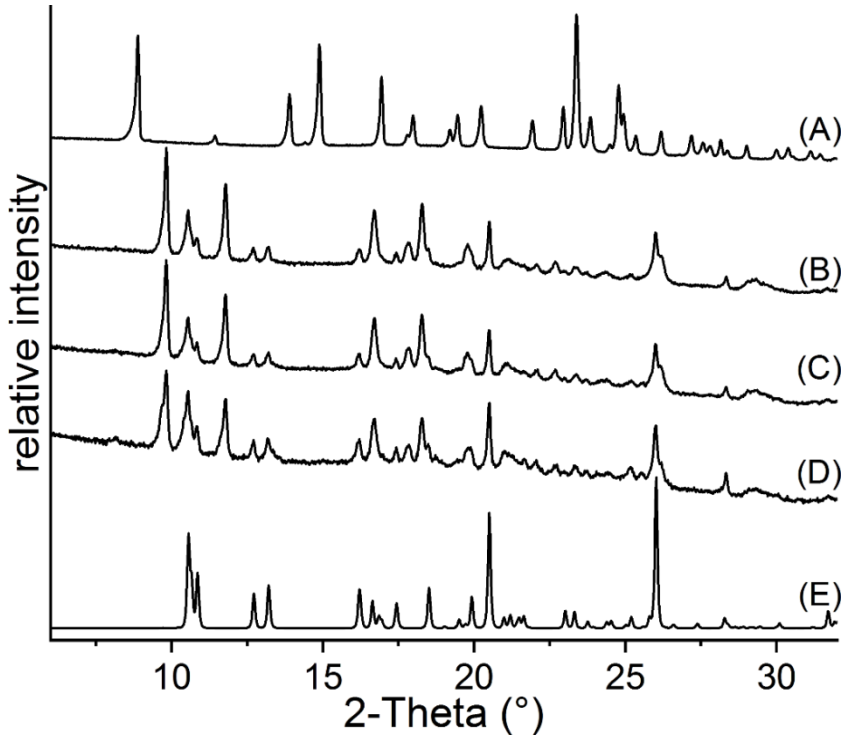

Figure S16. Calculated XRPD pattern for **2-Fe/H_2O** (A) and for **2-Fe/I** (E) together with the experimental pattern measured with Cu-Kα_1 radiation of samples obtained by heating **2-Fe/H_2O** at 75°C for 43h (B), 91h (C) and 10d (D).

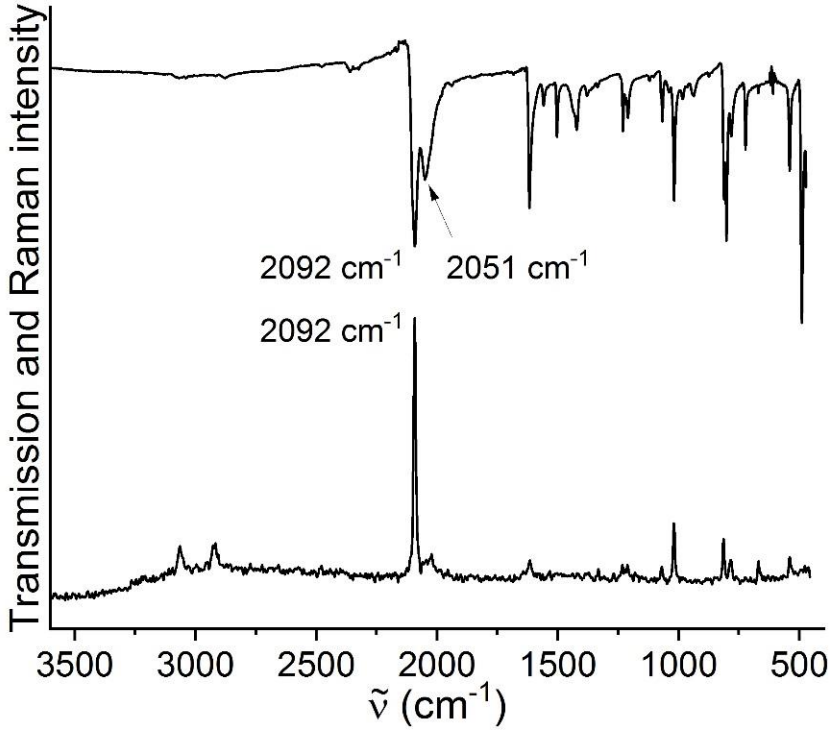

Figure S17. IR- (top) and Raman-spectra (bottom) of **2-Fe/II** with the values for the C-N stretching vibrations.

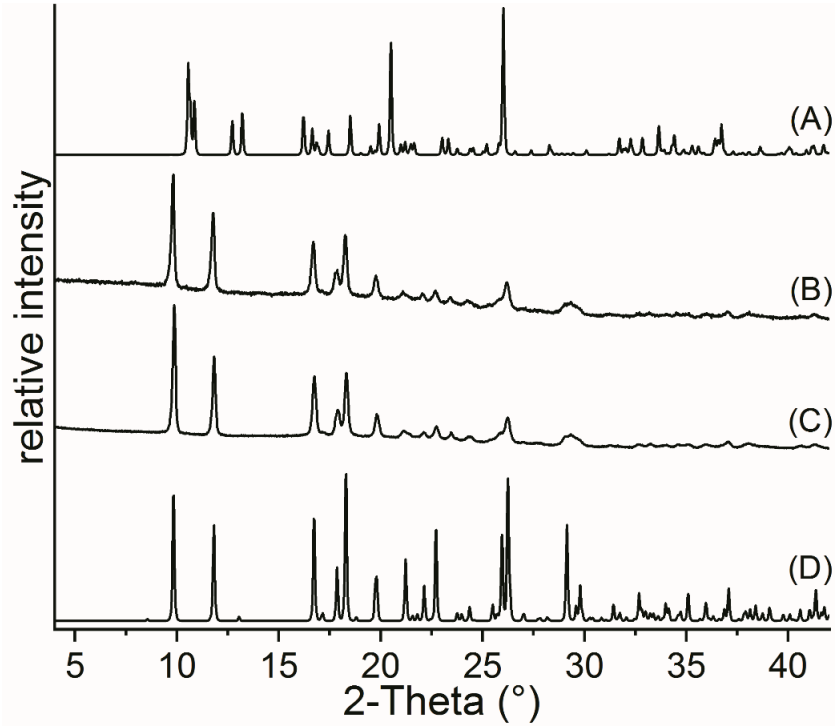

Figure S18. Calculated XRPD pattern for **2-Fe/I** (A) and **2-Fe/II** (D) and powder pattern of samples obtained by using a rotary evaporator to remove the water from **2-Fe/H_2O** (B and C).

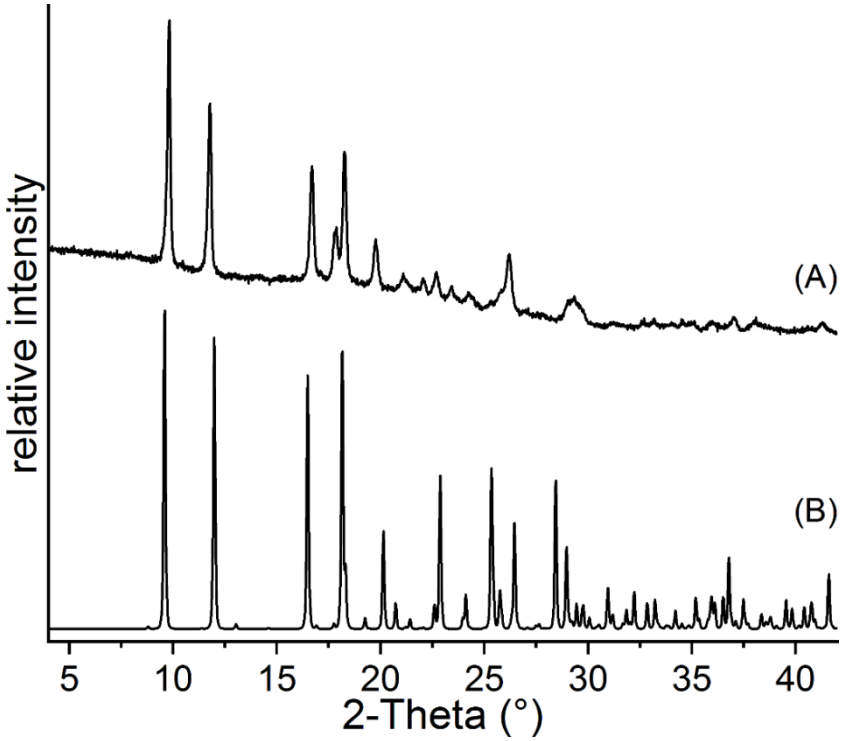

Figure S19. Experimental XRPD pattern of **2-Fe/II** measured with Cu-Kα_1 radiation obtained by evaporating H_2O from **2-Fe/H_2O** in a rotary evaporator (A) and calculated powder pattern for $[Cu(NCS)_2(4\text{-cyanopyridine})_2]_n$ (B).

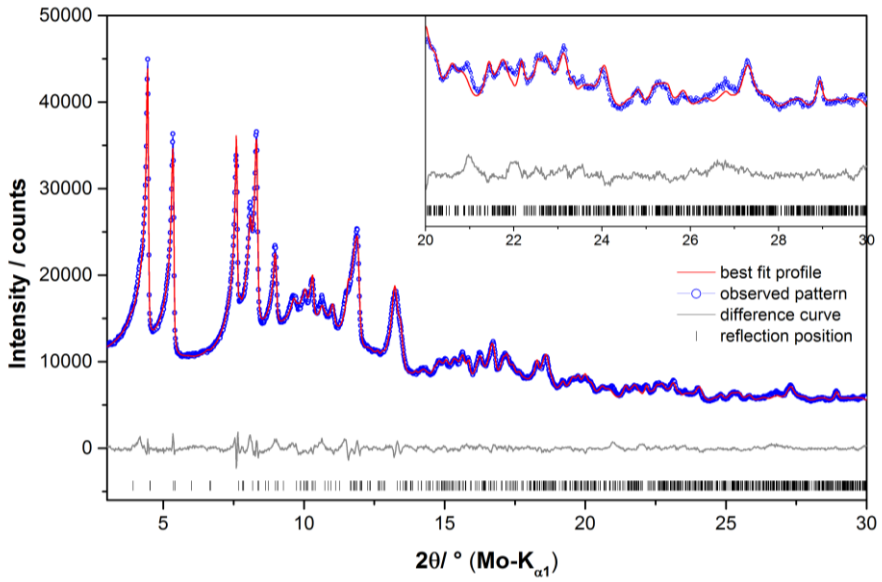

Figure S20. Rietveld plot of **2-Fe/II**. The observed pattern (circles) measured in Debye-Scherrer geometry, the best Rietveld fit profiles (line) and the difference curve between the observed and the calculated profiles (below) are shown. The high angle part starting at 25° in 2θ is enlarged for clarity.

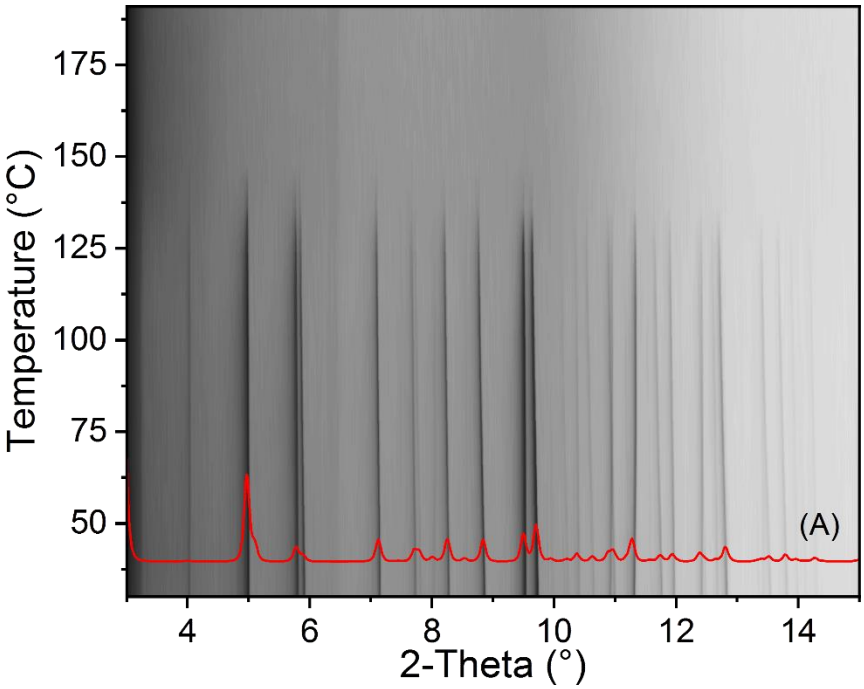

Figure S21. Experimental XRPD pattern of **1-Fe** measured as function of temperature measured with Mo-Kα radiation in an open capillary. As guide to the eye the calculated powder pattern of **1-Fe** is given in red.

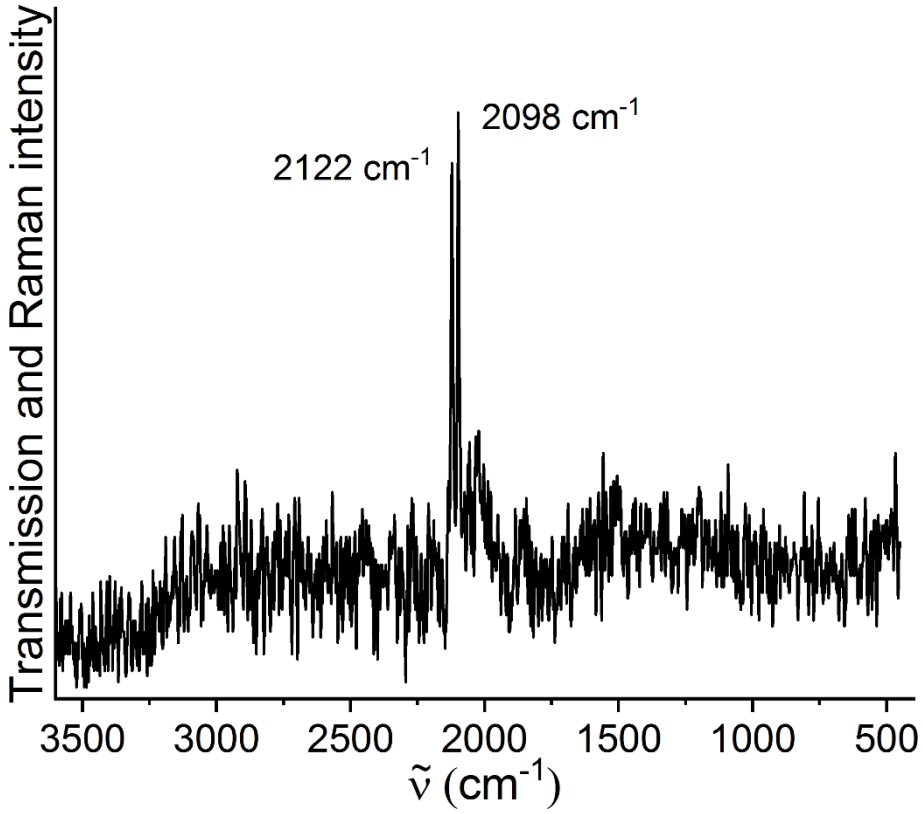

Figure S22. Raman-spectrum of **3-Fe** with the values for the CN-stretching vibrations.

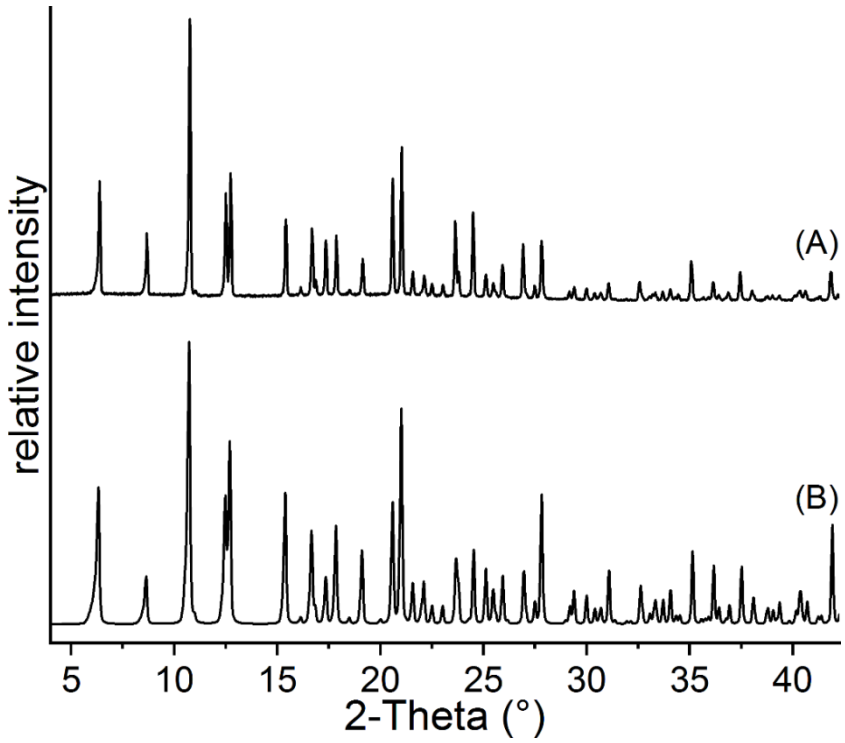

Figure S23. Experimental (A) and calculated (B) powder pattern of **1-Cd**.(Cu-Kα_1 radiation).

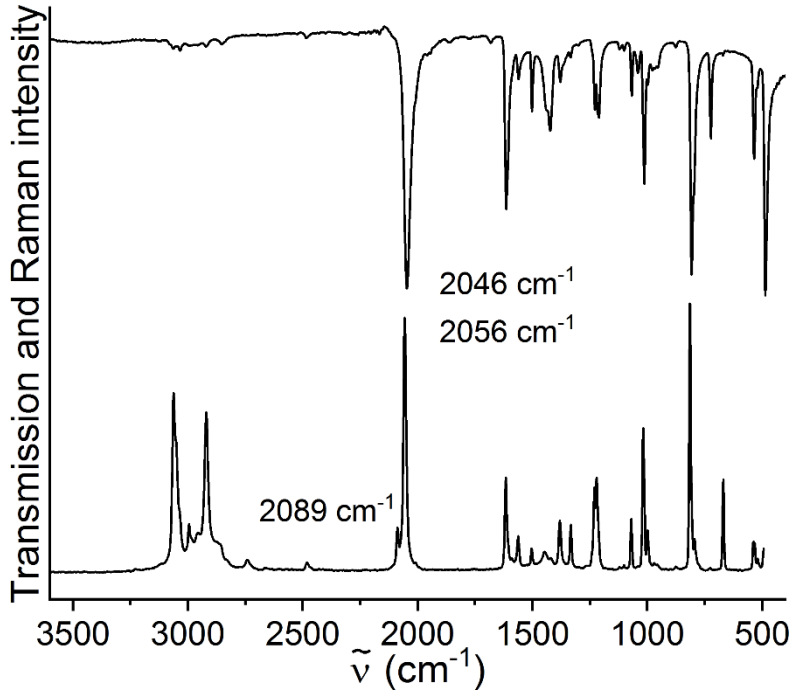

Figure S24. IR- (top) and Raman-spectra (bottom) of **1-Cd** with the values for the C-N stretching vibrations.

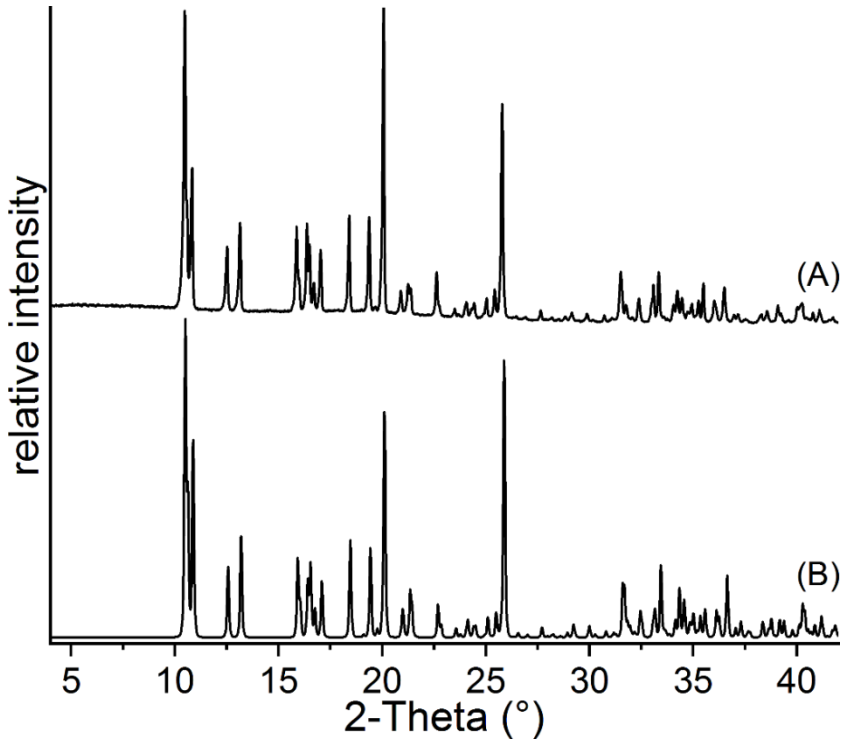

Figure S25. Experimental (A) and calculated (B) powder pattern of **2-Cd/I** (Cu-Kα_1 radiation).

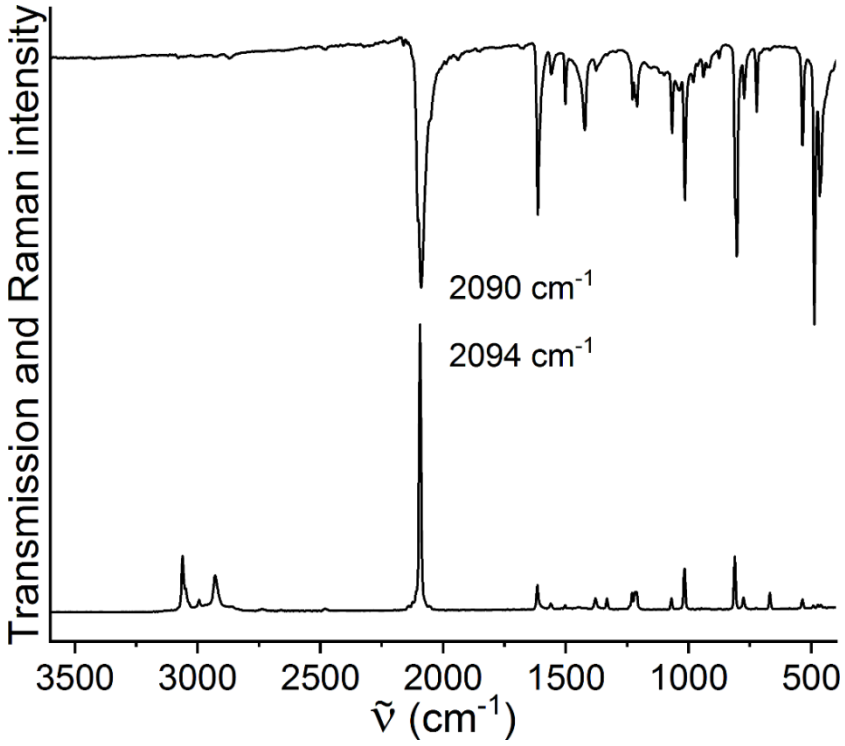

Figure S26. IR- (top) and Raman-spectra (bottom) of **2-Cd/I** with the values for the C-N stretching vibrations.

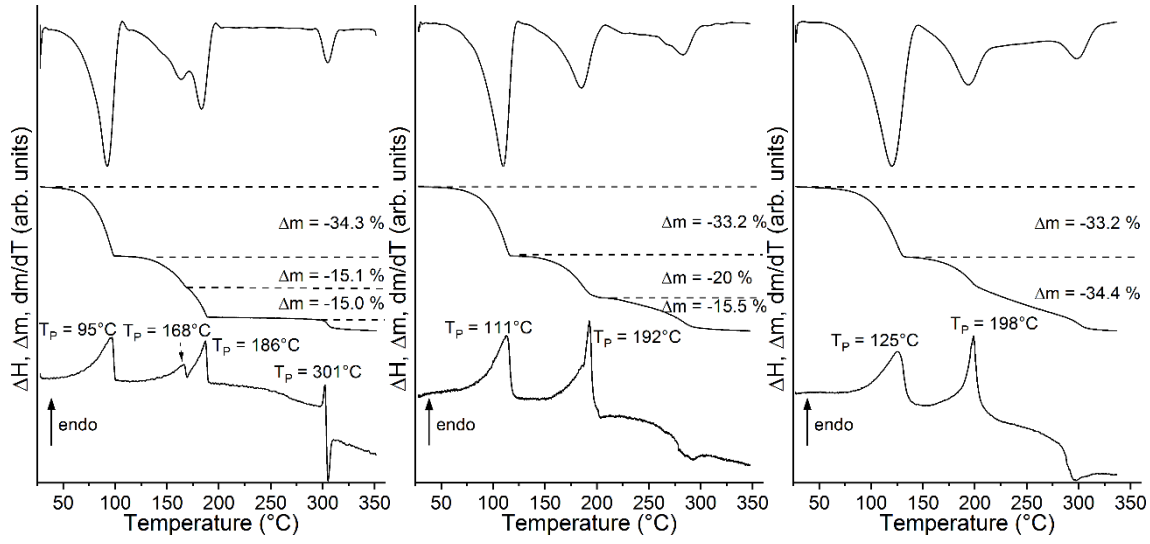

Figure S27. DTG, TG and DSC curves of **1-Cd** measured with 1°C/min, 4°C/min and 8°C/min (left to right). Given are the mass loss in percent and the peak temperatures (T_P).

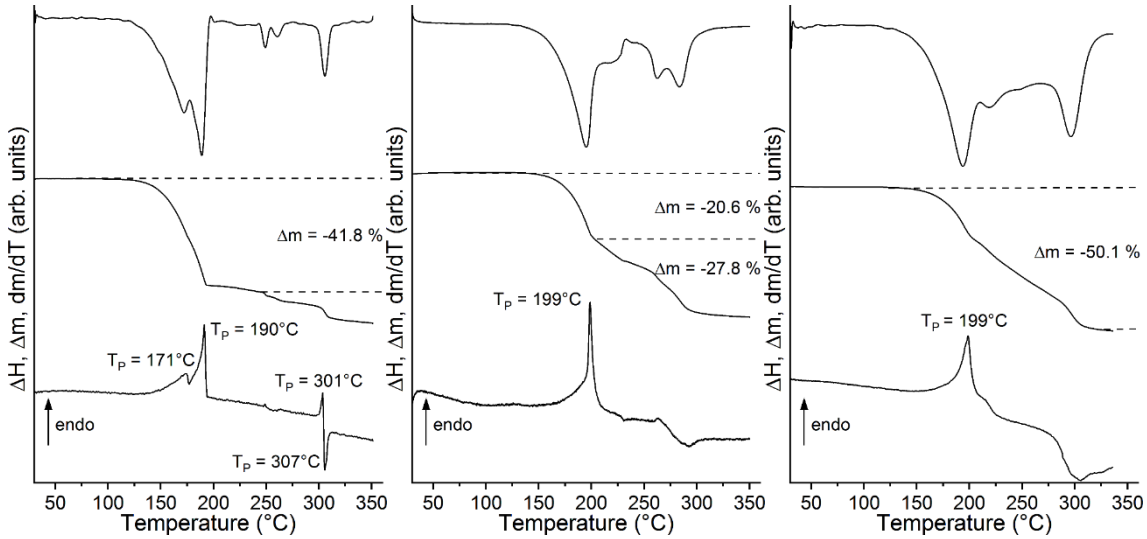

Figure S28. DTG, TG and DSC curves of **2-Cd/I** measured with 1°C/min, 4°C/min and 8°C/min (left to right). Given are the mass loss in percent and the peak temperatures (T_P).

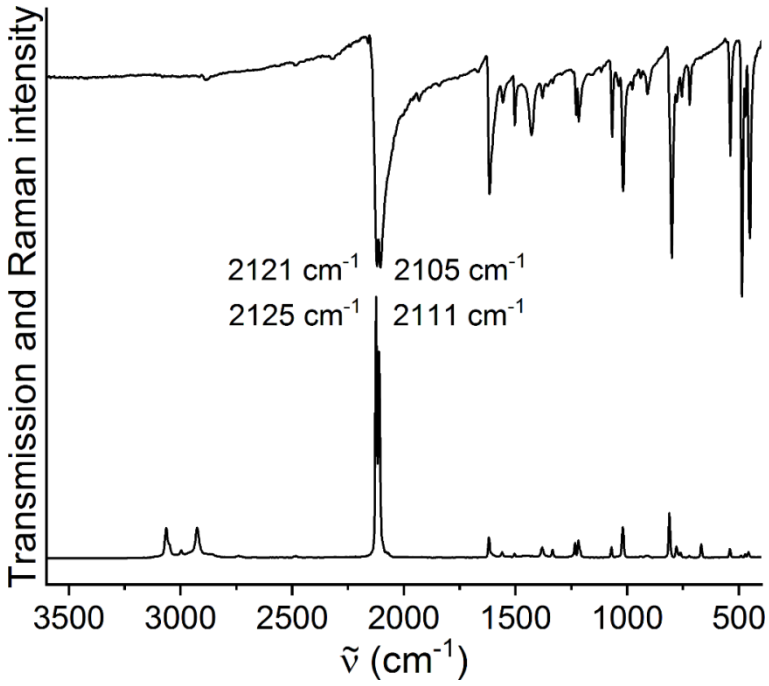

Figure S29. IR- (top) and Raman-spectra (bottom) of **3-Cd** with the values for the C-N stretching vibrations.

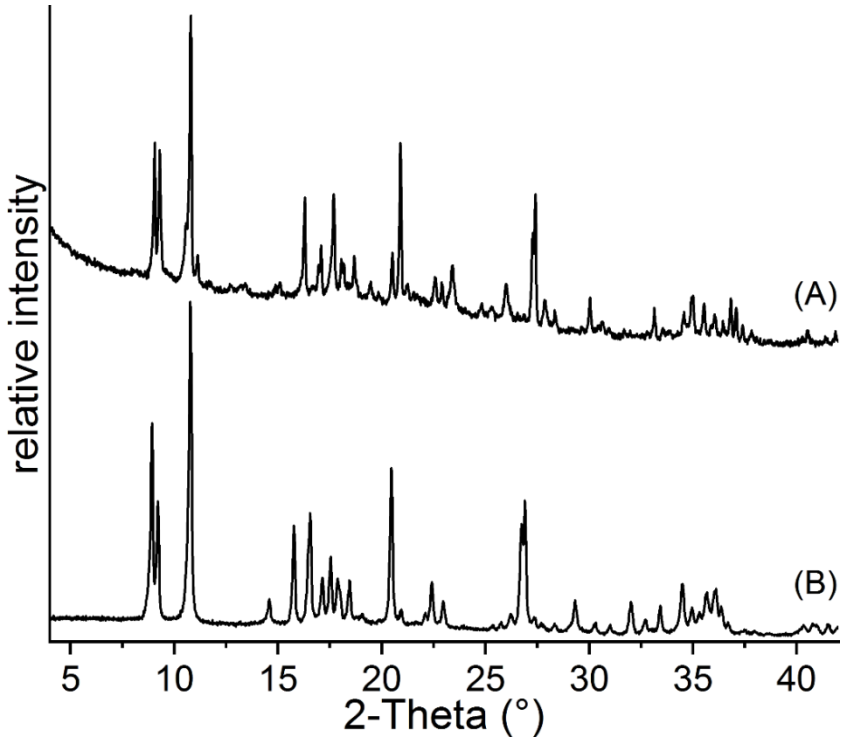

Figure S30. XRPD pattern of **3-Fe** (A) and of the residue obtained from the second step of **1-Cd** (B) measured with Cu-Kα_1 radiation.

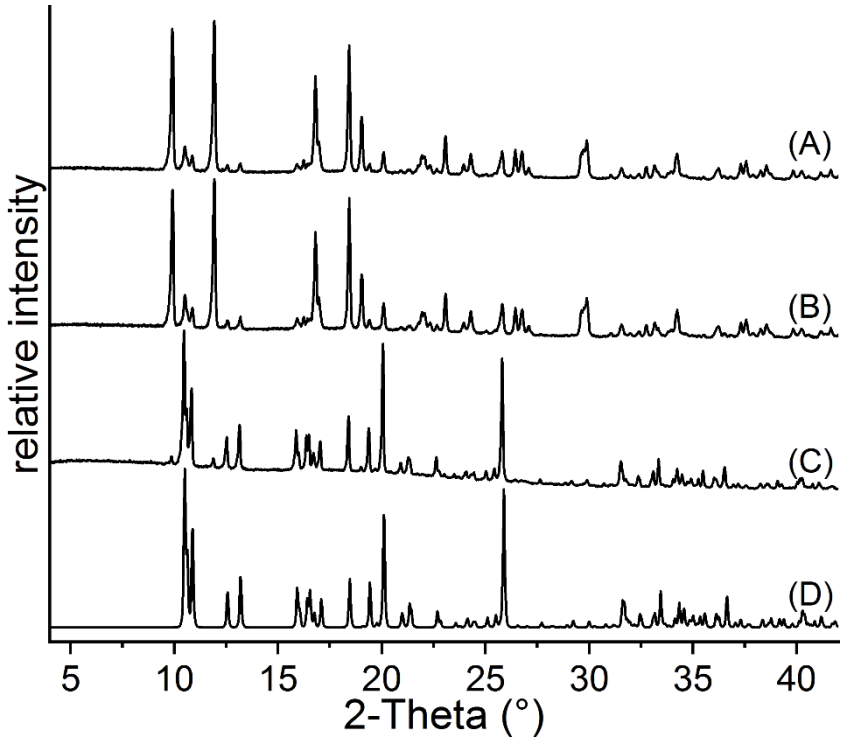

Figure S31. XRPD pattern (Cu-Kα_1 radiation) of the residues obtained in a TG measurement of **1-Cd** with a heating rate of 1°C/min directly after the first mass step (A) and at slightly higher temperatures (B) and isolated after the first mass step of a measurement at a heating rate of 8°C/min (C) and the calculated pattern of **2-Cd/I** (D).

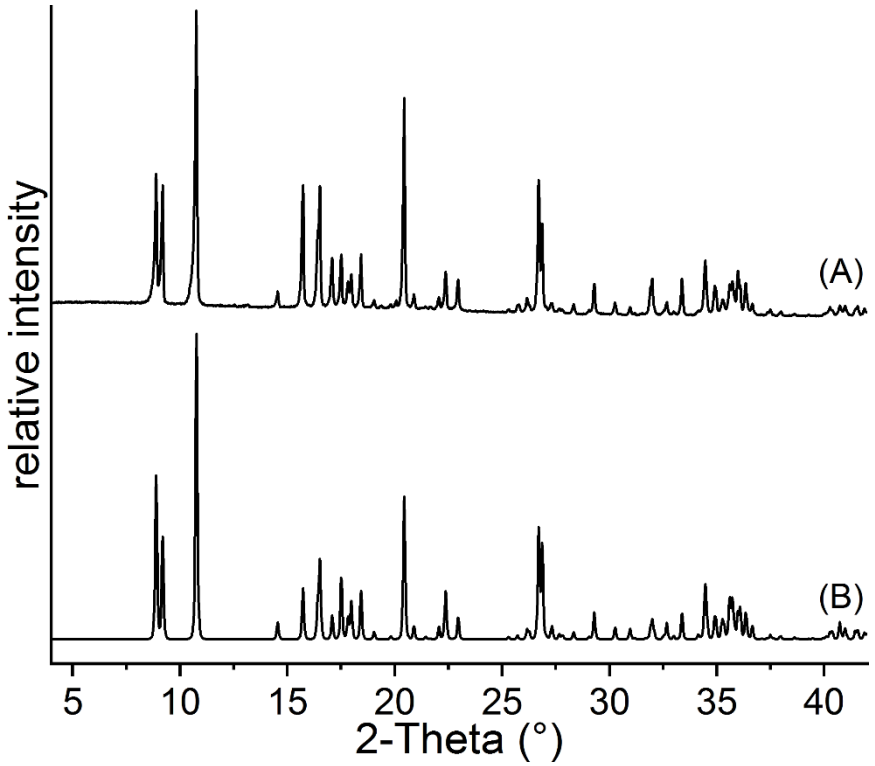

Figure S32. Experimental (A) and calculated powder pattern of **3-Cd** (B) measured with Cu-Kα_1 radiation.

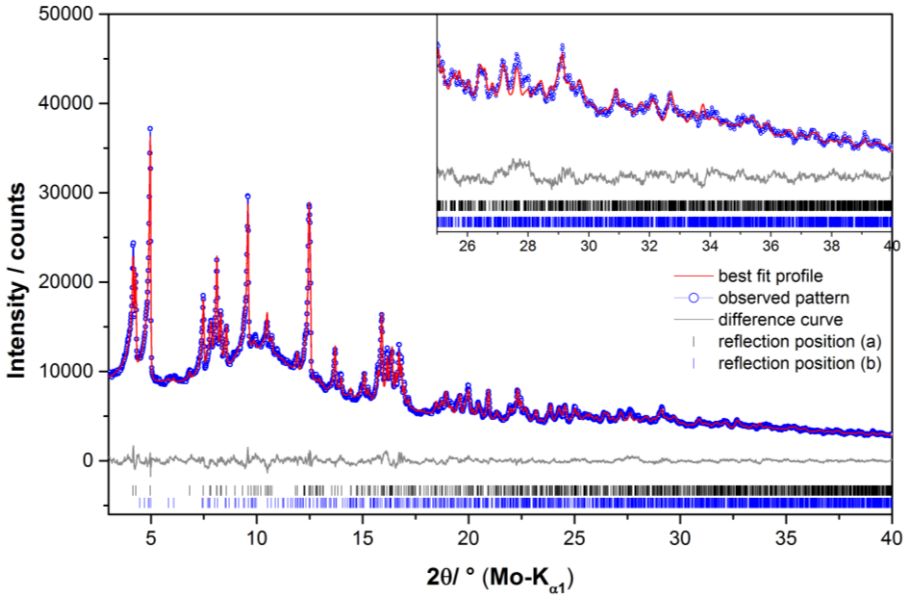

Figure S33. Rietveld plot for **3-Fe**. The observed pattern (blue circles) measured in Debye-Scherrer geometry, the best Rietveld fit profiles (red line), the difference curve between the observed and the calculated profiles (grey line) and calculated peak positions for $[Fe(NCS)_2(4\text{-picoline})]_n$ (black) and $[Fe(NCS)_2(4\text{-picoline})_2]_n$ (MOD2 - 2-Fe/I) (blue) are shown. The high angle part starting at 25° in 2θ is enlarged for clarity.

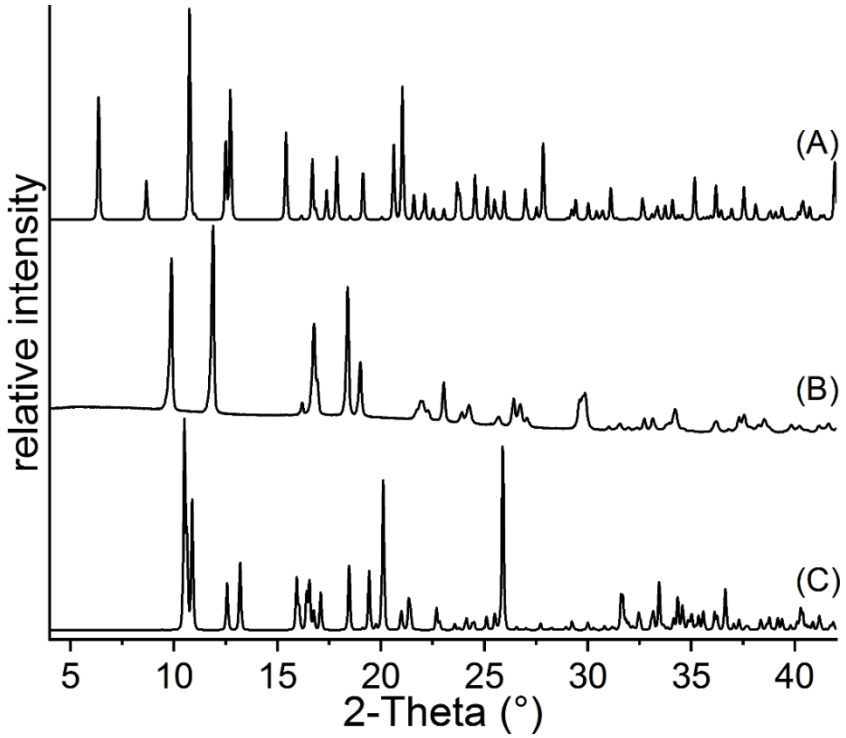

Figure S34. Calculated XRPD pattern of **1-Cd** (A) and of **2-Cd/I** (C) and experimental pattern of the crystalline sample obtained by crystallization under kinetic control (B) measured with Cu-Kα_1 radiation.

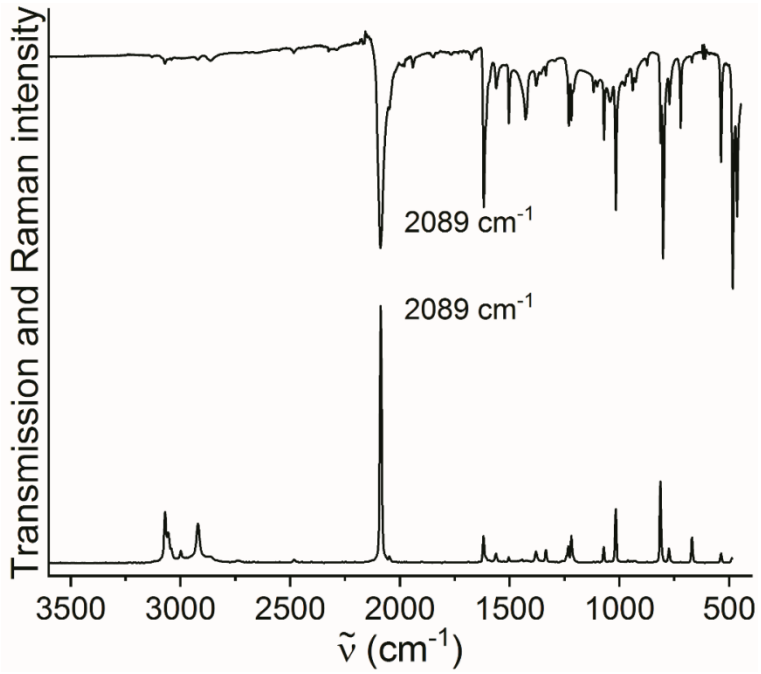

Figure S35. IR- (top) and Raman-spectra (bottom) from **2-Cd/III** with the values for the C-N stretching vibrations.

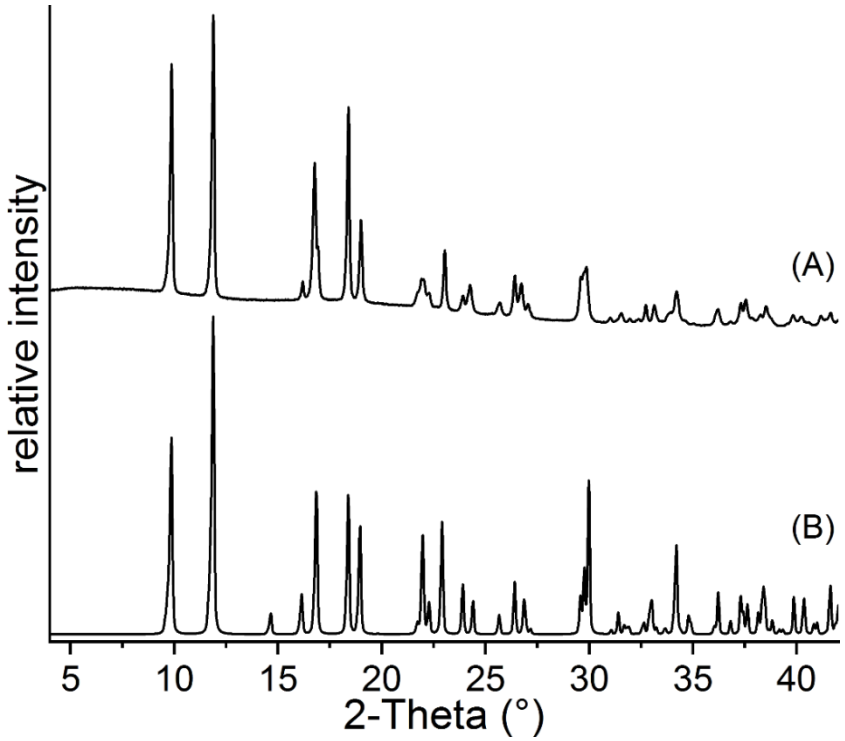

Figure S36. Experimental XRPD pattern (Cu-Kα_1 radiation) of **2-Cd/III** obtained by kinetically controlled synthesis (A) and calculated pattern of $[Cd(NCS)_2(4\text{-cyanopyridine})_2]_n$ (B).

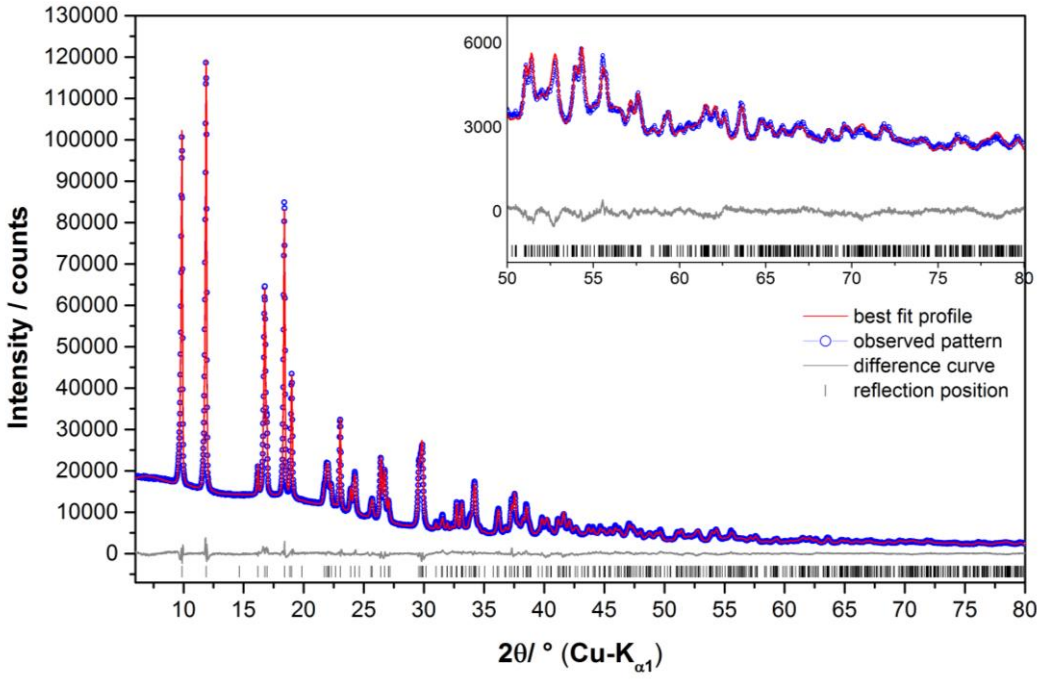

Figure S37. Rietveld plot of **2-Cd/III**. The observed pattern (blue circles) measured in Debye-Scherrer geometry, the best Rietveld fit profiles (red line), the difference curve between the observed and the calculated profiles (grey line) and calculated peak positions (black) are shown. The high angle part starting at 50° in 2θ is enlarged for clarity.

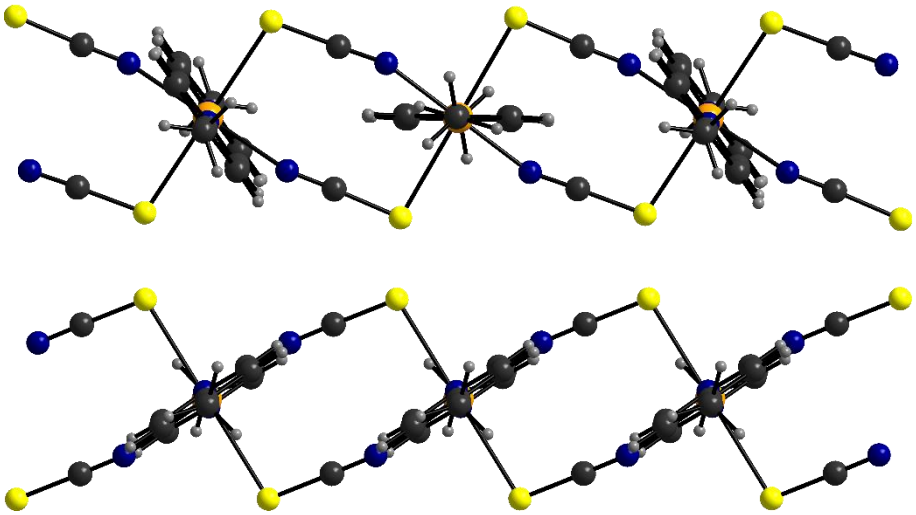

Figure S38. View on top of the chains of **2-Fe/II** (top) and **2-Cd/III** (bottom).

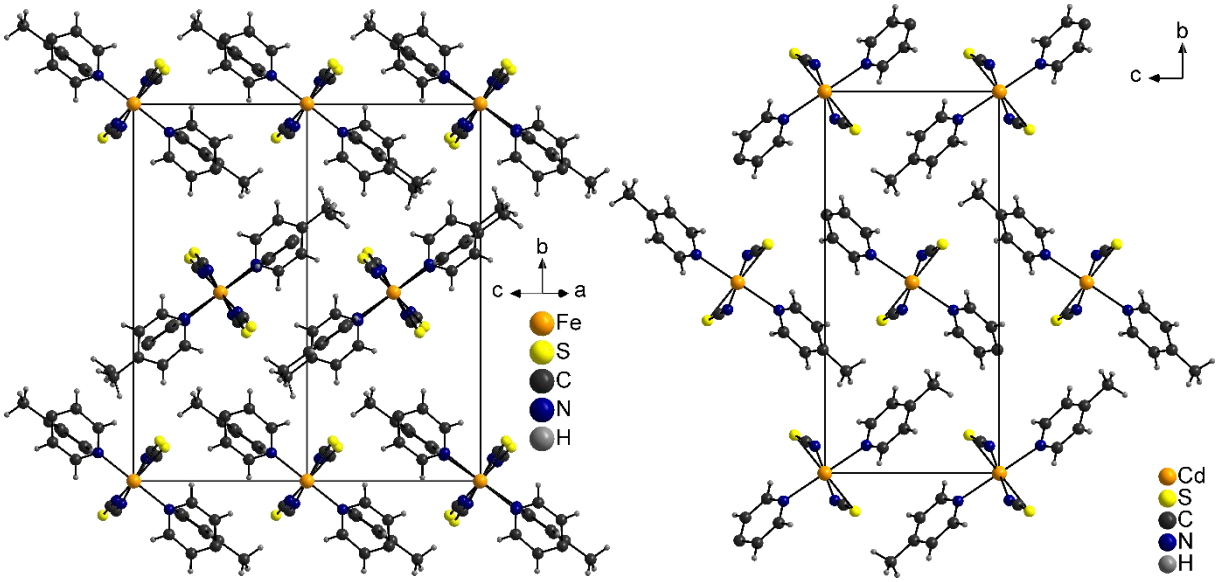

Figure S39. Packing diagram of **2-Fe/II** (left) and **2-Cd/III** (right) with view along the chains.

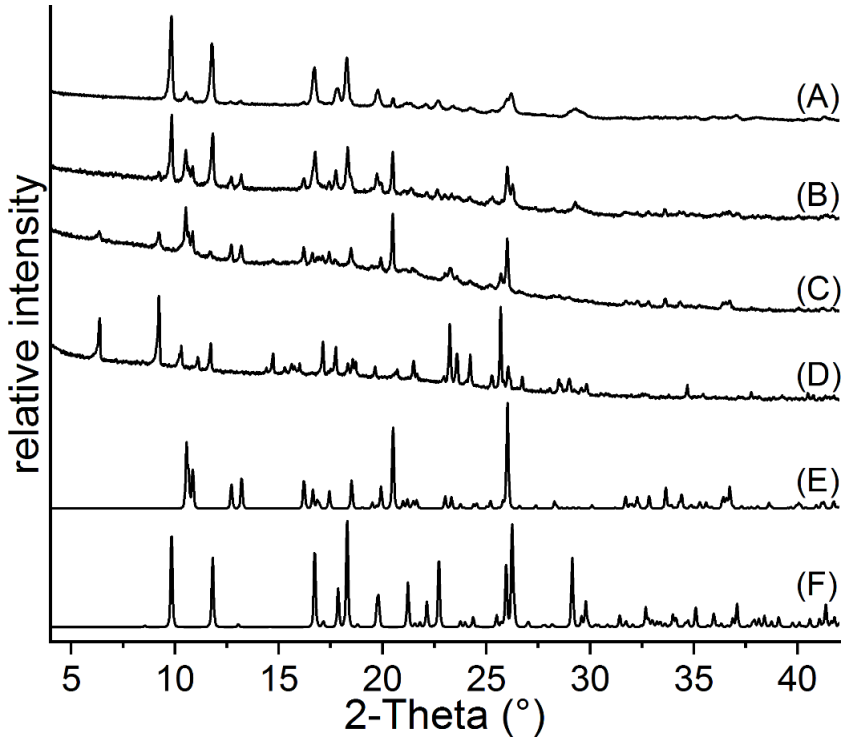

Figure S40. XRPD pattern of a mixture of **2-Fe/I** and **2-Fe/II** (A) which was stirred in a mixture of cyclohexane (1.5 mL) and MeCN (200 µL) for 1h (B), 1d (C) and 14d (D) measured with Cu-Kα_1 radiation together with the calculated powder pattern of **2-Fe/I** (E) and **2-Fe/II** (F).

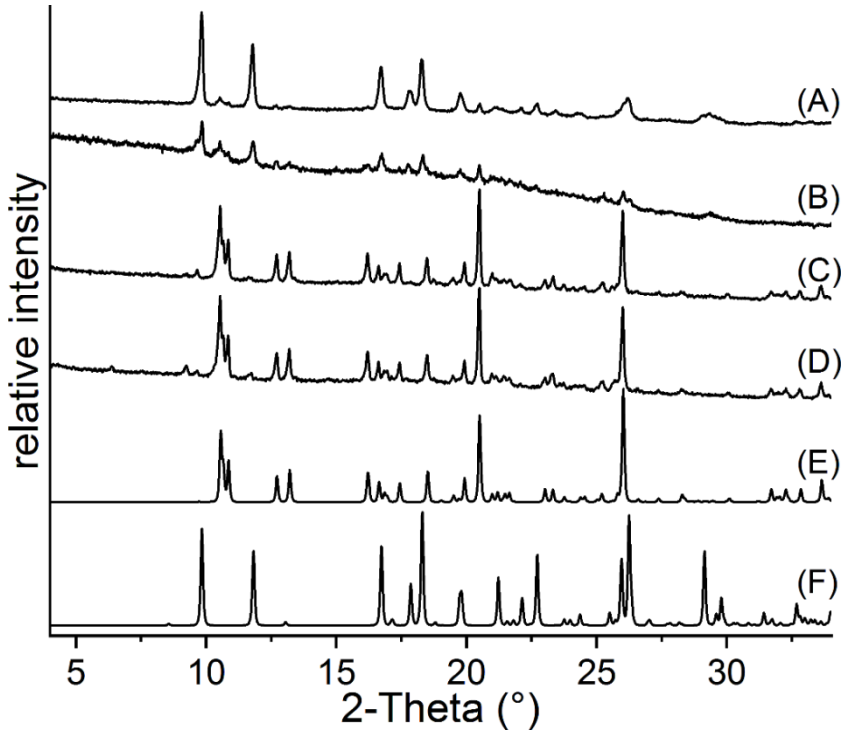

Figure S41. XRPD pattern of a mixture of **2-Fe/I** and **2-Fe/II** (A) which was stirred in a mixture of cyclohexane (2.0 mL) and EtOH (40 µL) for 1h (B), 1d (C) and 3d (D) together with the calculated powder pattern of **2-Fe/I** (E) and **2-Fe/II** (F) measured with Cu-Kα_1 radiation.

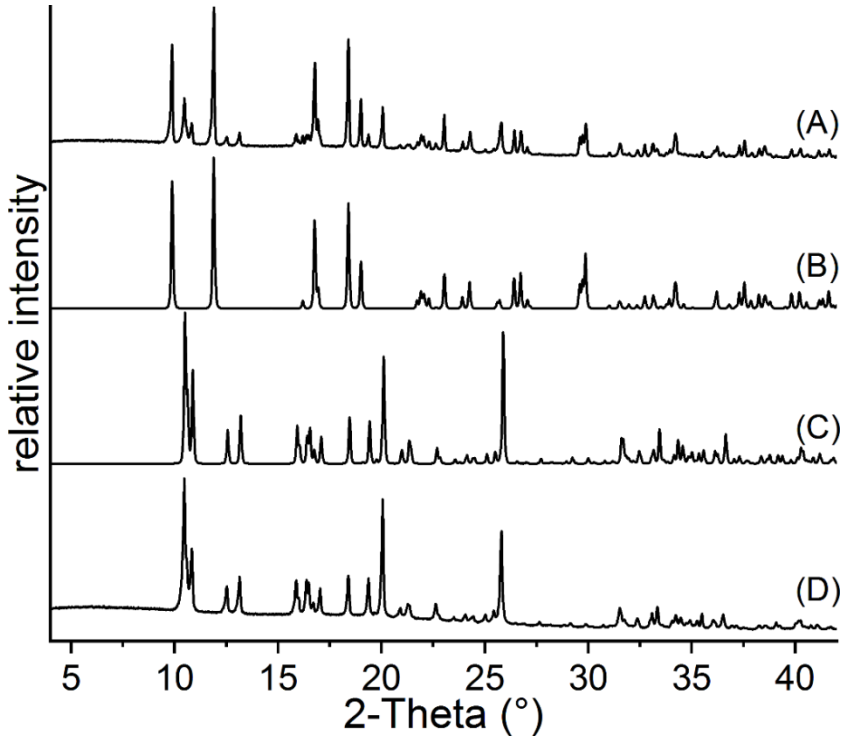

Figure S42. XRPD pattern of a mixture of **2-Cd/I** and **2-Cd/III** (A) and of this mixture stirred in MeOH for 15 min (D) measured with Cu-Kα_1 radiation together with the calculated powder pattern of **2-Cd/III** (B) and **2-Cd/I** (C).

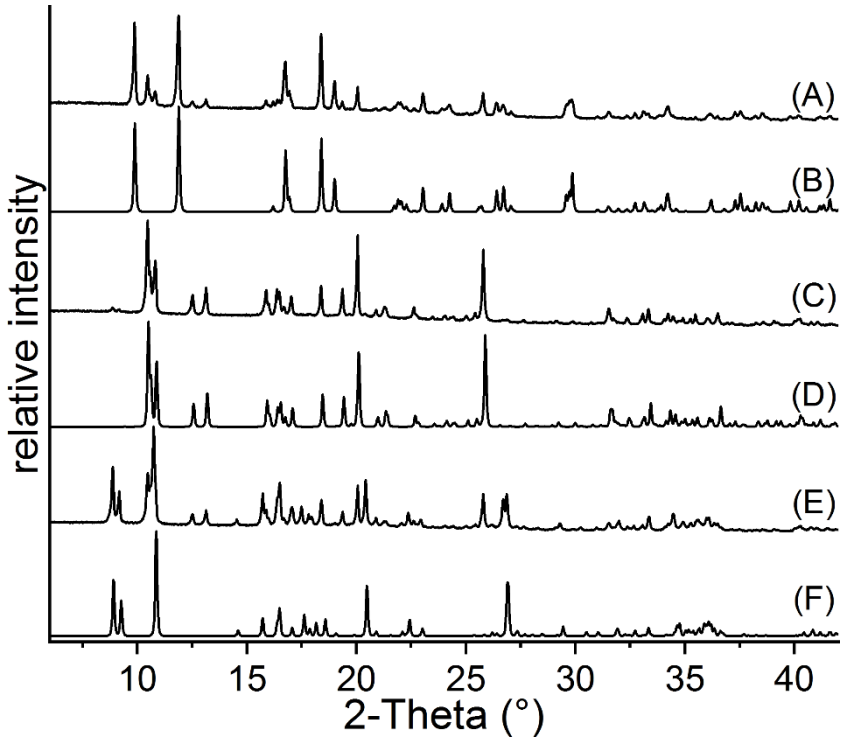

Figure S43. XRPD pattern (Cu-Kα_1 radiation) of the residues obtained by heating **2-Cd/III** to point 4 (A), point 5 (C) and point 6 (E; see Figure 6 in the manuscript) together with the calculated pattern of **2-Cd/III** (B), **2-Cd/I** (C) and of **3-Cd** (F).

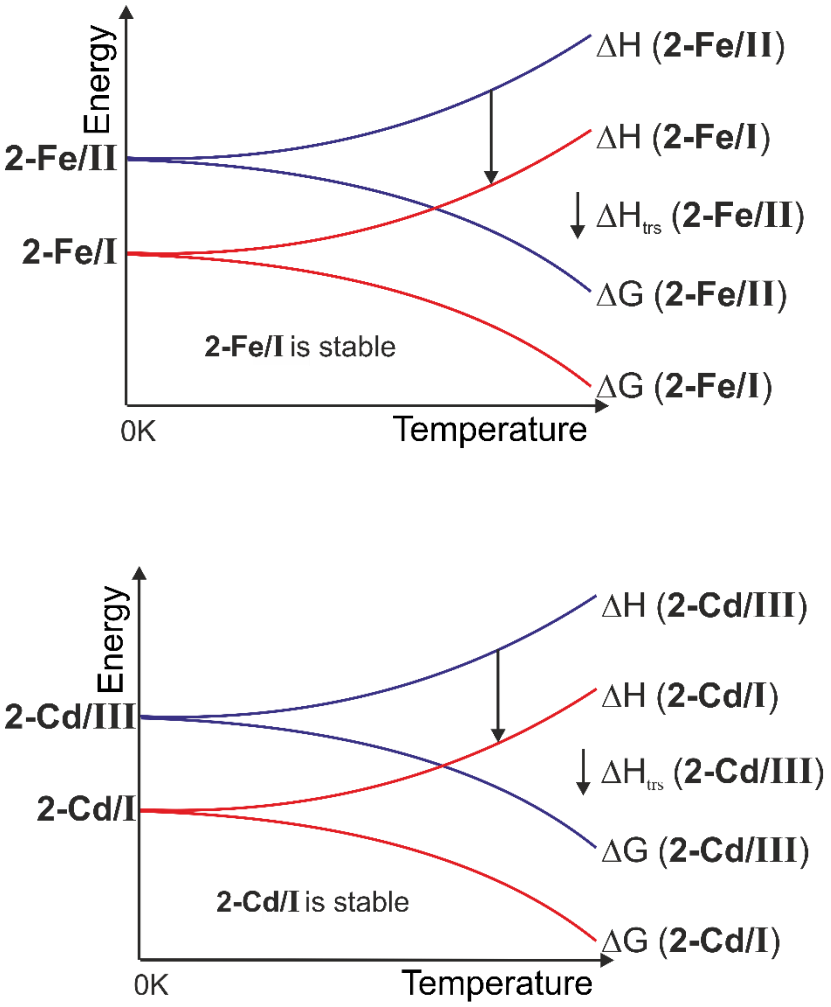

Figure S44. Energy-temperature diagram for **2-Fe/I** and **2-Fe/II** (top) and for **2-Cd/I** and **2-Cd/III** (bottom).

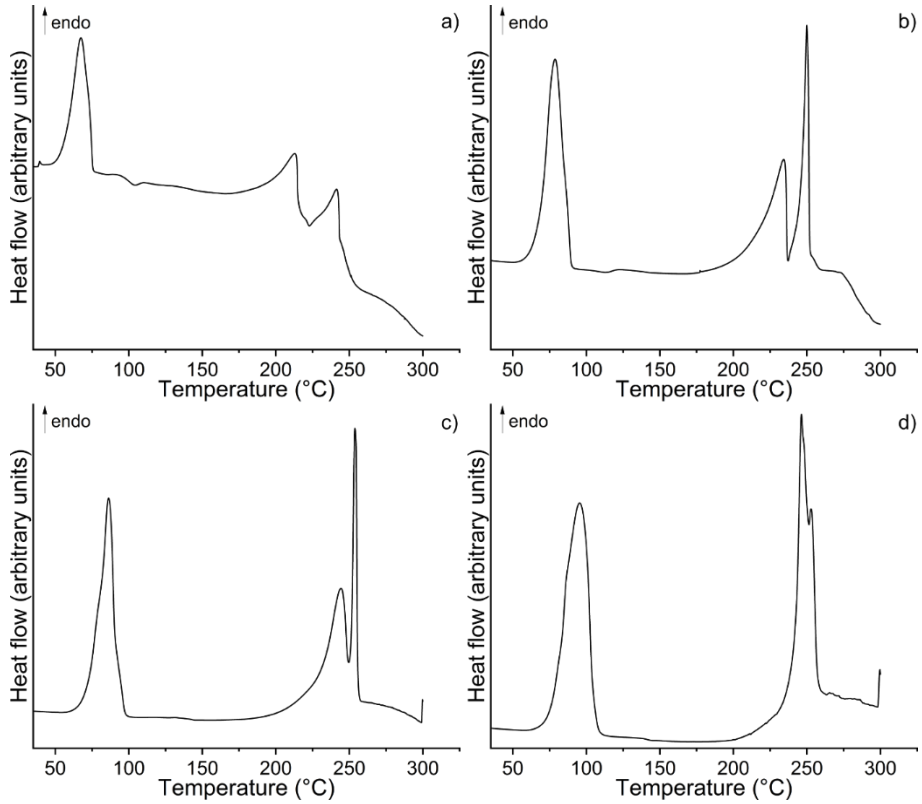

Figure S45. Heating rate dependent DSC measurements of **2-Fe/H_2O** with a) 1°C/min, b) 5°C/min, c) 10°C/min and d) 20°C/min.

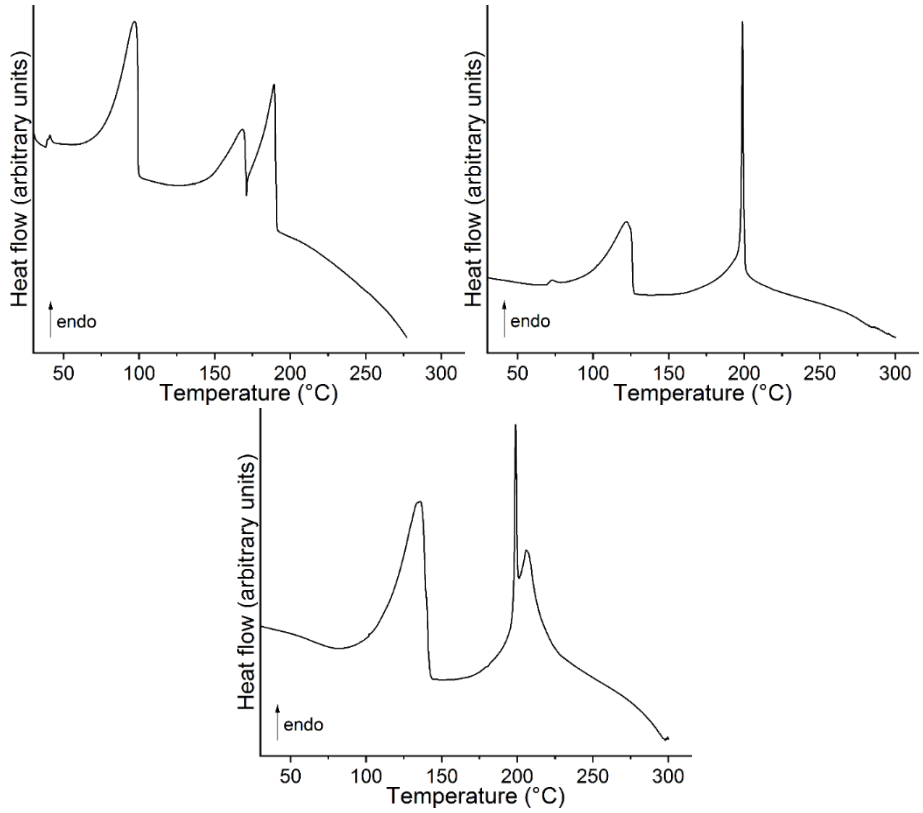

Figure S46. Heating rate dependent DSC measurements of **1-Cd** with heating rates of 1°C/min (top left), 5°C/min (top right) and 10°C/min (bottom left).

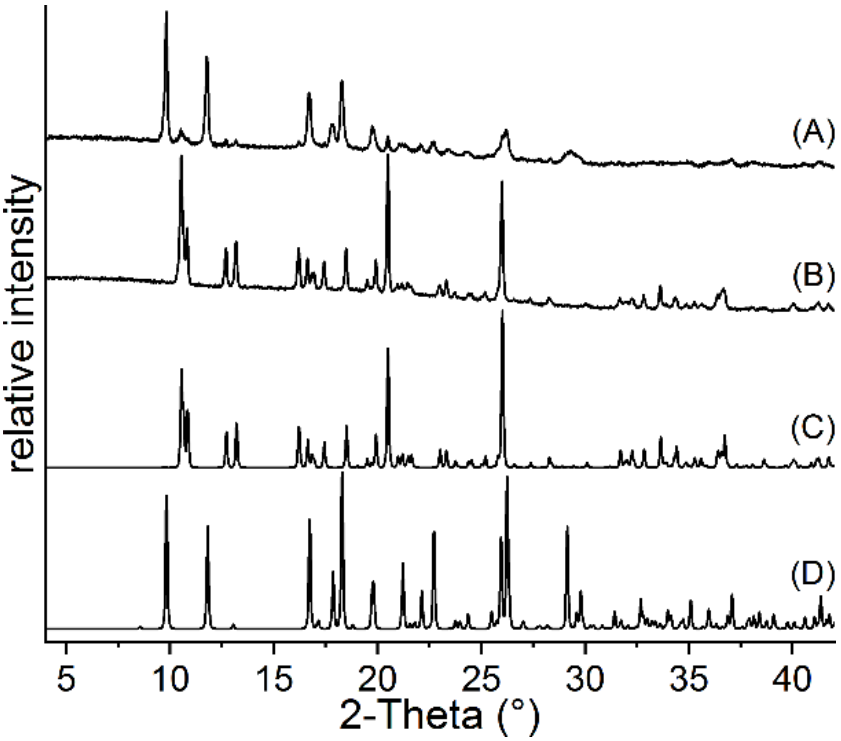

Figure S47. Experimental XRPD pattern of the residues obtained before (A) and after (B) the exothermic signal observed in a DSC measurement of **2-Fe/H_2O** with a heating rate of 1°C min measured with Cu-Kα_1 radiation and calculated pattern for **2-Fe/I** (C) and **2-Fe/II** (D).

Table S1. Selected crystal data and results of the structure refinements using single crystal data.

Compound	**1-Fe**	**3-Cd**
Sum formula	$C_{26}H_{28}FeN_6S_2$	$C_8H_7CdN_3S_2$
Molecular weight / g mol^{-1}	544.51	321.6957
Crystal system	trigonal	triclinic
Space group	$R\bar{3}$	$P\bar{1}$
Wavelength / Å	0.71073	0.71073
a / Å	27.693 (3)	5.8783 (5)
b / Å	27.693 (3)	10.3023 (10)
c / Å	11.1885 (10)	10.5662 (10)
α / °	90	71.108 (11)
β / °	90	78.415 (11)
γ / °	120	74.975 (11)
V / Å^3	7430.7 (17)	579.92 (11)
T / K	293	200
Z	9	2
D_{calc} / g cm^{-3}	1.095	1.842
μ / mm^{-1}	0.604	2.21
Crystal size / mm	0.08 x 0.06 x 0.04	0.11 x 0.08 x 0.07
Data collection	IPDS 2	IPDS 1
Absorption correction	numerical	numerical
θ_{max}	25.1	27.504
Refl. collected	7472	8372
Unique refl.	2951	2609
R_{int}	0.043	0.083
Refl. [$F_o > 4\sigma(F_o)$]	1855	2268
parameters	160	164
$R_1[F_o > 4\sigma(F_o)]$	0.0676	0.036
wR_2 (for all data)	0.171	0.091
GOF	1.04	1.003
T_{min}, T_{max}	0.9192, 0.9606	0.6013, 0.7991
$\Delta\rho_{max}$, $\Delta\rho_{min}$ / eÅ^{-3}	0.480 and -0.312	0.684 and -1.639

Table S2. Selected crystal data and results of the Rietveld refinements.

Compound	**2-Fe/H_2O**	**2-Fe/I**	**2-Fe/II**	**3-Fe**	**2-Cd/III**
Sum formula	$FeC_{14}H_{18}O_2N_4S_2$	$FeC_{14}H_{14}N_4S_2$	$FeC_{14}H_{14}N_4S_2$	$FeC_8H_7N_3S_2$	$CdC_{14}H_{14}N_4S_2$
Molecular weight / g mol^{-1}	394.30	358.26	358.26	265.11	414.82
Crystal system	monoclinic	monoclinic	monoclinic	triclinic	monoclinic
Space group	$P2_1/c$	$C2/c$	$P2_1/c$	$P\bar{1}$	$P2_1/n$
Wavelength/ Å	0.7093	0.7093	0.7093	0.7093	1.5406
a / Å	10.2833(6)	20.2576(8)	11.2197(16)	5.6544(4)	5.83966(12)
b / Å	12.3146(6)	9.3191(3)	17.949(2)	10.3052(8)	17.8924(4)
c / Å	7.6860(3)	19.2831(6)	9.0538(12)	10.4498(7)	8.6365(2)
α / °	90	90	90	70.083(5)	90
β / °	103.823(4)	116.135(2)	112.712(7)	78.969(7)	108.751(2)
γ / °	90	90	90	75.518(4)	90
V / $Å^3$	945.12(8)	3268.1(2)	1681.9(4)	550.52(7)	854.49(3)
T / K	298	298	298	298	298
Z	2	8	4	2	2
refined parameters	40	59	50	55	47
D_{calc} / g cm^{-3}	1.371	1.456	1.415	1.581	1.612
R_{wp} / % [a]	3.82	2.23	2.44	3.12	2.76
R_p / % [a]	2.97	1.68	1.91	2.50	2.00
R_{Bragg} / % [a]	2.18	0.98	0.68	1.46	1.72
Starting angle measured / ° 2 ϑ	2	2	2	2	3
Final angle measured / ° 2 θ	50	50	50	50	80
Starting angle used / ° 2 θ	2	2	3	2	6
Final angle used / ° 2 θ	40	40	30	40	80
Step width (° 2 θ)	0.015	0.015	0.015	0.015	0.015
Time / hrs	16	16	16	16	6